Optimal Energy Procurement for Geo-distributed Data Centers in Multi-timescale Markets

Submission Type: Research

Abstract

Multi-timescale electricity markets augment the traditional electricity market by enabling consumers to procure electricity in a future market. Heavy power consumers, such as cloud providers and data center operators, can significantly benefit from multi-timescale electricity markets by purchasing some of the needed electricity ahead of time at cheaper rates. However, the energy procurement strategy for data centers in multi-timescale markets becomes a challenging problem when real world dynamics, such as spatial diversity of data centers and uncertainties of renewable energy, IT workload, and electricity price, are taken into account. In this paper, we develop energy procurement algorithms for geo-distributed data centers that utilize multi-timescale markets to minimize the electricity procurement cost. We propose two algorithms. The first algorithm provides provably optimal cost minimization, while the other achieves near-optimal cost at a much lower computational cost. We empirically evaluate our energy procurement algorithms using real world traces of renewable energy, electricity prices, and the workload demand. Our empirical evaluations show that our proposed energy procurement algorithms save up to 44% of the total electricity cost compared to traditional algorithms that do not use multi-timescale electricity markets and geographical load balancing.

1 Introduction

Data centers are becoming the largest and the fastest growing consumers of electricity in the United States. It is reported that US data centers consumed 91 billion kilowatt-hours (kWh) in 2013, which is more than twice of the electricity consumed by households in New York City (see [39]). In the same report, the electricity consumption of the data centers is estimated to reach 140 billion kWh in 2020 due to the explosion of demand from cloud computing and other Internet-scale services. Global cloud providers, such as Google and Amazon, who operate multiple data centers spend billions of dollars annually on their electricity bills [32].

Multi-timescale electricity markets have been proposed to improve the efficiency of electricity markets [12]. Multi-timescale electricity markets encompass both *forward* (futures) and *spot* (real-time) markets. While energy is procured at the time of consumption in a spot market, forward markets allow customers to buy electricity a day ahead or even several months ahead of when it is consumed. Forward electricity markets reduce the risk for both the supplier and consumer by reducing the quantity of energy trading in the real-time spot markets [4]. Furthermore, purchasing electricity ahead of time can facilitate the expansion of renewable energy sources (RESs). For example, Google invested in purchasing renewable energy from renewable project developers for 20 years [15].

Utilizing multi-timescale markets has great potential for electricity cost savings for cloud providers who operate one or more data centers. There has been much recent work that exploit the variation of real-time electricity prices in the temporal and spatial dimensions to reduce the total electricity cost. For example, prior papers show how a cloud provider can exploit real-time electricity prices in multiple market locations and move load to locations with a cheaper price [32, 10, 33]. Other papers exploit temporal variation in the real-time energy price and use energy storage to reduce the electricity costs [17, 18, 40], i.e., the storage device is charged during the times when the electricity price is low and discharged for use when the price is high. However, while prior work focus on traditional real-time markets, the potential for using multi-timescale market for electricity cost reduction has not been studied in the context of a cloud provider and is the topic of our paper.

Our focus on using forward markets to lower the electricity cost for a cloud provider is challenging for multiple reasons. The optimal amount of electricity that a cloud provider should purchase for time slot t for each location in a forward market at T_l time slots ahead depends on the workload, the availability of onsite renewables, and the real-time electricity price at t at that location. The main challenge is that the future workloads, renewables and real-time electricity prices are not perfectly predictable and are subject to significant forecasting er-

rors. Note that if the cloud provider is too conservative and buys too less from the forward market, any shortfall in electricity would need to be covered by purchasing it from the more expensive[1] real-time market. Likewise, if the cloud provider is too aggressive and buys too much from the forward market, any excess in electricity will go wasted. In addition, the ability of a cloud provider to move load from one data center to another, possibly incurring a performance penalty that we characterize as the "delay cost", adds an additional level of complexity that needs to be optimized. In this work, we provide an optimization framework for tackling the aforementioned challenges.

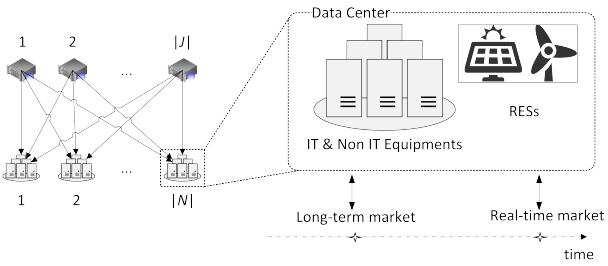

Figure 1: Geo-distributed data centers in long-term and real-time markets.

1.1 Our contributions

In this paper, we focus on designing an energy procurement system to provision geo-distributed data centers in multi-timescale markets. Our contributions are three-fold.

(1) Algorithm development. We develop two algorithms for a cloud provider with geo-distributed data centers to buy electricity in multi-timescale markets: one algorithm provides provable optimality guarantees, while the other is simpler, uses limited predictions but achieves near-optimal performance. To develop the energy procurement system, we model the problem of procuring electricity for geo-distributed data centers in multi-timescale markets in Section 2. The system model is general and applicable to any global cloud provider with access to multi-timescale electricity markets. We focus on two-timescale markets that consists one long-term market and one real-time market, though our model and algorithms can be extended to handle multiple markets at various timescales. We present the characteristics of the objective functions and the optimal solution in Section 3. The two algorithms that we design, prediction based algorithm (PA) and stochastic gradient based algorithm (SGA), are described in Section 5. Both algorithms seek to minimize the total operating cost of the cloud provider across all data centers. While PA is simple and performs very well, SGA provably achieves the optimal solution.

(2) Predictability analysis using real-world traces. We collect and analyze real world traces of PV generation, wind generation, electricity prices, and IT workload demand, using these traces as inputs for our energy procurement algorithms. A detailed data analysis of real world traces of PV generation, wind generation, electricity prices, and workload, is presented in Section 4. The data analysis not only enables us to evaluate our algorithms using real-world data, but also provides insights into the nature of prediction errors. To procure electricity in forward markets, the energy procurement system needs to predict the renewable generation, workload, and electricity prices in real-time. Therefore, we focus on addressing the following questions. What are the properties of the real world data? What do the distributions of prediction errors look like? How correlated are prediction errors in the spatial domain?

(3) Empirical Evaluation. We carry out a detailed empirical evaluation of our proposed energy procurement systems. In Section 6, we demonstrate that SGA can converge to the optimal solution in a small number of iterations. Moreover, we show that PA, our heuristic algorithm, surprisingly achieves a near-optimal solution. Some intuitions behind this are the trade-off between energy cost and delay cost, and the independence among prediction errors. The proposed energy procurement systems are compared with other plausible energy procurement strategies to highlight their benefits. The impact of renewable energy and prediction errors on the proposed systems are also fully explored.

2 Model

2.1 System model

Two-timescale markets. A service provider operating geo-distributed data centers can purchase electricity in two markets – a long-term market and a real-time market. Note that electricity is consumed at time $t = 0$ must be procured at time $t = 0$ in the real-time market, but needs to be procured *ahead of time* at time $t = -T_l$ in the long-term market.

Geo-distributed data centers. We consider a set N of geo-distributed data centers serving workload demands from a set J of sources as illustrated in Figure 1. The workload demand from each source is routed to some of the $|N|$ data centers. Here, a source can represent the aggregate demand from a group of local users, such users of a particular city, ISP, or geographical region. Each data

[1]In some cases, the prices in the forward markets might be (on average) higher than real-time prices. If so, instead of saving electricity expenditure, the cloud provider can participate in forward markets to reduce cost variations. Our model can be extended to handle either case.

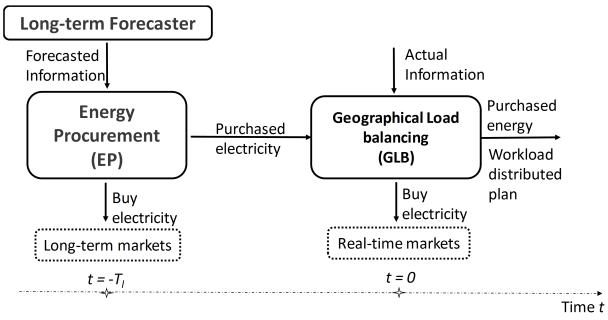

Figure 2: Energy Procurement System (EPS) Architecture for geo-distributed data centers.

center has access to renewable energy sources (RESs). Further, each data center participates in a (local) long-term electricity market and a (local) real-time electricity market. In other words, each data center i can buy electricity ahead of time in its long-term market, and can also buy additional electricity in its real-time market if necessary. Also, note that different data centers may buy from different markets that are locally available to them.

Energy procurement system (EPS). Our proposed energy procurement system for geo-distributed data centers is depicted in Figure 2. There are three main components, namely, the long-term forecaster component, the energy procurement (EP) component and the geographical load balancing (GLB) component. The long-term forecaster provides the foretasted information for the energy procurement. The forecasted information includes the predicted values and the prediction error distributions of IT workload, renewable energy generations, and electricity prices. We design the algorithms for the long-term forecaster in Section 4. The EP component buys electricity for each data center in the corresponding long-term markets (at time $t = -T_l$) based on the electricity prices in the long-term markets and forecasts of real-time prices, workload, and renewable generation. The GLB component (at time $t = 0$) distributes the realized workload from sources to data centers and purchases additional electricity as needed in the real-time markets.

Data center. Let M_i denote the number of servers in data center i. The actual number of active servers at in real-time(at time $t = 0$) (real-time) is denoted by m_i. In practice, there can be more than a hundred thousand servers in one data center. Thus, in our mathematical modeling, we treat m_i as a real number satisfying $0 \leq m_i \leq M_i$.

At $t = 0$, the power consumption of data center i is denoted by d_i^r. In general, the power consumption of data center i is dependent on the number of active servers m_i and the workload arrival λ_i. Let $d_i^r = O_i(m_i, \lambda_i)$, where the power consumption function $O_i(\cdot)$ is non-decreasing in m_i and λ_i. To model the power consumption, we apply the right-sizing technique for data center power management which only switches on the necessary number of servers at their peak power to serve to the workload arrival, and put the unused servers to sleep [23]. Hence the power consumption of the data center is proportional to the number of active servers. For theoretical analysis, we assume that $d_i^r = m_i$ in which the power consumptions of server are normalized and homogeneous. ~~This model is simple but general, and can be applied to other cases. For example, it can be applied to the~~ linear power consumption model [34, 26, 24].

Workload. Workload demand from source j in real-time ($t = 0$) is denoted as L_j^r. We assume that the exact realization of the random vector $\boldsymbol{L}^r = (L_j^r, j \in J)$ is known to the cloud provider at time $t = 0$, and is an input to GLB. Let λ_{ij} denote the distributed workload arrival from source j to data center i at time $t = 0$ (set by GLB). Thus,

$$\sum_{i \in N} \lambda_{ij} = L_j^r \qquad (j \in J),$$

$$\sum_{j \in J} \lambda_{ij} = \lambda_i \qquad (i \in N).$$

Workload balancing among data centers has been proposed in literature to reduce the energy cost for cloud providers [32, 33, 26, 8].

Renewable energy. Data centers can utilize their integrated RESs. Let w_i^r denote the renewable energy generation at data center i in real-time ($t = 0$). We assume that the exact realization of the random vector $\boldsymbol{w}^r = (w_i^r, i \in N)$ is known at time $t = 0$, and is an input to GLB.

Electricity price. For each data center i, the cloud provider can purchase electricity at time $t = -T_l$ in the local long-term market and then purchase any additional electricity needed in the local real-time market at time $t = 0$. Let p_i^l denote the long-term price for 1 unit of electricity at data center i at time $t = -T_l$, and p_i^r be the real-time price for data center i at time $t = 0$. We assume that $\boldsymbol{p}^l = (p_i^l, i \in N)$ is fixed (or equivalently, is known at the time of the long-term procurement), and $\boldsymbol{p}^r = (p_i^r, i \in N)$ is a random vector whose exact value is known is known at time $t = 0$ and is an input to GLB.

Note that the real-time workload $\boldsymbol{L}^r$, the real-time renewable generation $\boldsymbol{w}^r$, and the real-time electricity prices $\boldsymbol{p}^r$ are unknown at the time of the long-term procurement by the EP component, but are known at the time of operation of the GLB component. We assume that the distributions of renewable energy, workload, and electricity prices are continuous. In addition, all the w_i^r, L_j^r, and p_i^r are assumed to be bounded random variables.

2.2 Cost model

The total cost of operating geo-distributed data centers in composed of a delay cost and an energy cost. The delay cost is the monetary cost incurred due to the delay in processing the arriving workload at time $t = 0$. The energy cost is the net electricity cost in both long-term and real-time markets.

Delay cost. The delay cost represents the monetary cost incurred due to the delay experienced by the sources. There could be several ways to model the delay cost based on the responsive time. In particular, the lost revenue can be proportional to a certain range of delay [5]. Thus, we model the delay cost $h_{ij}(m_i, \lambda_i)$ of routing and processing each unit of workload from source j to data center i as follows:

$$h_{ij}(m_i, \lambda_i) = \beta\left(\frac{1}{\mu_i - \lambda_i/m_i} + \pi_{ij}\right) \qquad (i \in N, j \in J)$$

where the parameter β weighs the delay relative to the monetary cost. The first term above captures queuing delay at delay center i, which is based on the well-known average queuing model, called M/GI/1 processor sharing queue. The second term captures the network delay from source j to data center i. Here, μ_i is the service rate of servers in data center i. We require that

$$\lambda_i \le m_i \mu_i \qquad (i \in N).$$

Energy cost. Let q_i^l and q_i^r respectively denote the amount of electricity purchased in the long-term market and the real-time market by data center i. Of course, we require that sufficient electricity is procured to process the workload routed to each data center, i.e.,

$$q_i^r + w_i^r + q_i^l \ge m_i \quad (i \in N).$$

The electricity costs of data center i in the long-term market and the real-time market are respectively computed as

$$R_i^l(q_i^l) = p_i^l q_i^l \qquad i \in N,$$
$$R_i^r(q_i^r) = p_i^r q_i^r \qquad i \in N.$$

2.3 Formulation of optimal energy procurement in multi-timescale markets

In this section, we describe the optimization formulation for optimal energy procurement. Recall that the total cost of operating geo-distributed data centers in our two-timescale market setting is the sum of the energy cost and the delay cost, given by

$$F = \sum_{i \in N} R_i^l(q_i^l) + \sum_{i \in N} R_i^r(q_i^r) + \sum_{i \in N, j \in J} \lambda_{ij} h_{ij}(m_i, \lambda_i).$$

We seek to minimize $\mathbb{E}[F]$ subject to the aforementioned constraints. Note that this optimization is performed on two timescales, with different sets of information available ~~at~~ each. The EP component optimizes the long-term procurements $\boldsymbol{q}^l = (q_i^l, i \in N)$ given only distributional information of the real-time workload $\boldsymbol{L}^r$, the real-time renewable generation $\boldsymbol{w}^r$, and the real-time electricity prices $\boldsymbol{p}^r$. The GLB component optimizes the workload routing $\boldsymbol{\lambda} = (\lambda_{ij}, i \in N, j \in J)$, the number of active servers $\boldsymbol{m} = (m_i, i \in N)$ at the data centers, and the real-time procurements $\boldsymbol{q}^r = (q_i^r, i \in N)$ given the prior long-term procurements $\boldsymbol{q}^l$, and the exact realization of $(\boldsymbol{p}^r, \boldsymbol{L}^r, \boldsymbol{w}^r)$. Below, we first formalize the real-time optimization, followed by the long-term optimization.

Geographical load balancing in real-time markets. Note that ~~at~~ real-time, GLB optimizes the real-time procurements $\boldsymbol{q}^r$, the numbers of active servers $\boldsymbol{m}$, and the workload routing $\boldsymbol{\lambda}$, given the long-term procurements $\boldsymbol{q}^l$ and the realization of the random vector $(\boldsymbol{p}^r, \boldsymbol{L}^r, \boldsymbol{w}^r)$. The total cost as seen by GLB is

$$F^r(\boldsymbol{q}^r, \boldsymbol{m}, \boldsymbol{\lambda}, \boldsymbol{p}^r) := \sum_{i \in N} R_i^r(q_i^r) + \sum_{i \in N, j \in J} \lambda_{ij} h_{ij}(m_i, \lambda_i).$$

Thus, the real-time optimization is defined as follows.

$$\textbf{GLB-RT:} \min_{\boldsymbol{m}, \boldsymbol{\lambda}, \boldsymbol{q}^r} F^r(\boldsymbol{q}^r, \boldsymbol{m}, \boldsymbol{\lambda}, \boldsymbol{p}^r)$$

s.t.

$$\lambda_{ij} \ge 0 \quad \forall i \in N, j \in J \tag{1a}$$
$$\sum_{i \in N} \lambda_{ij} = L_j^r \quad \forall j \in J \tag{1b}$$
$$\lambda_i \le m_i \mu_i, \quad \forall i \in N \tag{1c}$$
$$0 \le m_i \le M_i \quad \forall i \in N \tag{1d}$$
$$q_i^r \ge 0, \quad \forall i \in N \tag{1e}$$
$$m_i - q_i^r - w_i^r \le q_i^l \quad \forall i \in N, \tag{1f}$$

Since $p_i^r \ge 0$, it easily follows that any solution of the above optimization problem satisfies $q_i^r = [m_i - w_i^r - q_i^l]_+$, where $[x]_+ := \min\{0, x\}$. Thus, the real-time objective can be re-written as

$$\tilde{F}^r(\boldsymbol{q}^l, \boldsymbol{m}, \boldsymbol{\lambda}, \boldsymbol{p}^r, \boldsymbol{w}^r) = \textstyle\sum_{i \in N} p_i^r [m_i - w_i^r - q_i^l]_+ + \sum_{i \in N, j \in J} \lambda_{ij} h_{ij}(m_i, \lambda_i). \tag{2}$$

With this notation, GLB-RT can be equivalently expressed as follows.

$$\min_{\boldsymbol{m}, \boldsymbol{\lambda}} \tilde{F}^r(\boldsymbol{q}^l, \boldsymbol{m}, \boldsymbol{\lambda}, \boldsymbol{p}^r, \boldsymbol{w}^r)$$

s.t.

$$(\boldsymbol{m}, \boldsymbol{\lambda}) \in C(L^r).$$

Here, the convex compact set $C(L^r)$ is defined by the constraints (1a)–(1e).

GLB-RT problem is a convex optimization problem and hence can solved efficiently using standard techniques [7]. For instance, CVX (Matlab Software for Disciplined Convex Programming) tool [16] can be used to solve GLB-RT. In Section 3.2, we prove several interesting properties of the optimal solutions of GLB-RT.

Energy procurement in long-term markets. At time $t = -T_l$, the cloud provider purchases electricity $\boldsymbol{q}^l$ in long-term markets that will be used at real-time. Note that optimzation of the long-term procurements has to be performed based only on distributional information for the random vector $(\boldsymbol{p}^r, \boldsymbol{L}^r, \boldsymbol{w}^r)$, and subject to the real-time optimization that will be subsequently performed based on the realization of the random vector $(\boldsymbol{p}^r, \boldsymbol{L}^r, \boldsymbol{w}^r)$.

Let us denote the optimal value of the optimization GLB-RT by $F^{*r}(\boldsymbol{q}^l, \boldsymbol{p}^r, \boldsymbol{L}^r, \boldsymbol{w}^r)$. The long-term objective is thus defined as

$$F^l(\boldsymbol{q}^l) := \sum_{i \in N} R_i^l(q_i^l) + \mathbb{E}\left[F^{*r}(\boldsymbol{q}^l, \boldsymbol{p}^r, \boldsymbol{L}^r, \boldsymbol{w}^r)\right].$$

Note that the above expectation is with respect to the random vector $(\boldsymbol{p}^r, \boldsymbol{L}^r, \boldsymbol{w}^r)$. The long-term optimization problem is then given by:

$$\textbf{EP-LT:} \ \min F^l(\boldsymbol{q}^l)$$
$$\text{subject to}$$
$$\boldsymbol{q}^l \in \mathbb{R}_+^N$$

The above optimization is more challenging than GLB-RT. In Section 3.1, we prove that EP-LT is a convex optimization and characterize the gradient of the objective function. These results are then used to ~~arrive at a~~ provably optimal stochastic gradient algorithm in Section 5.

3 Characterizing the Optima

In this section, we present characterizations of the optimal solutions to EP-LT and GLB-RT, which are important for understanding the behavior of the energy procurement system, and also for proving convergence of the stochastic gradient algorithm in Section 5.

3.1 Characterizations of EP-LT

Our first result is that EP-LT is indeed a convex optimization, which suggests that EP-LT is a tractable optimization.

Theorem 1. *$F^l(\boldsymbol{q}^l)$ is convex over $\boldsymbol{q}^l \in \mathbb{R}_+^N$.*

We provide the proof of Theorem 1 in Appendix A.1. Next, we characterize the gradient of the EP-LT objective function as follows.

Theorem 2. *The gradient of $F^l(\cdot)$ is characterised as ~~follows.~~*

$$\frac{\partial F^l(\boldsymbol{q}^l)}{\partial q_i^l} = p_i^l + \mathbb{E}\left[\frac{\partial F^{*r}(\boldsymbol{q}^l, \boldsymbol{p}^r, \boldsymbol{L}^r, \boldsymbol{w}^r)}{\partial q_i^l}\right]$$
$$= p_i^l - \mathbb{E}\left[\varrho_i(\boldsymbol{q}^l, \boldsymbol{p}^r, \boldsymbol{L}^r, \boldsymbol{w}^r)\right],$$

where $\varrho_i(\boldsymbol{q}^l, \boldsymbol{p}^r, \boldsymbol{L}^r, \boldsymbol{w}^r)$ is the unique Lagrange multiplier of GLB-RT corresponding to the constraint (1f)*.*

Note that the first equality in the theorem statement asserts that the order of an expectation and a partial derivative can be interchanged. The second equality relates the partial derivative of F^{*r} with respect to q_i^l to a certain Lagrange multiplier of GLB-RT. We provide the proof of Theorem 2 in Appendix A.2.

We note that Theorem 2 does not enable us to compute the gradient of the $F^l(\cdot)$ exactly. Indeed, the expection the Lagrange multiplier ϱ_i with respect to $(\boldsymbol{p}^r, \boldsymbol{L}^r, \boldsymbol{w}^r)$ would in general be analytically intractable. However, Theorem 2 does enable a noisy estimation of the gradient of the $F^l(\cdot)$ via Monte Carlo simulation as follows. Suppose we simulate a finite number, say $\mathbb{S}$, of samples from the distribution of $(\boldsymbol{p}^r, \boldsymbol{L}^r, \boldsymbol{w}^r)$. In practice, we can obtain these samples by using real-world traces as is done in Section 4. For each sample, the Lagrange multipliers $(\varrho_i, i \in N)$ can be computed efficiently by solving GLB-RT. By averaging the $\mathbb{S}$ instances of $(\varrho_i, i \in N)$ ~~thus~~ obtained, we ~~get~~ an unbiased estimate of the gradient of $F^l(\cdot)$. This in turn enables us to solve EP-LT using a stochastic gradient descent method; details follow in Section 5.

3.2 Characterizations of GLB-RT

~~To begin, it~~ is easy to see that GLB-RT has at least one optimal solution. Although the optimal solution is generally not unique, there are natural aggregate quantities that are unique over the set of optimal solutions, which is a convex set. The optimal solutions preserve the uniqueness and sparsity properties of GLB as in existing works [26, 25]. The uniqueness of optimal solutions say that the server arrival rate, $\bar{\lambda}_i = \lambda_i / m_i$, is common across all optimal solutions. It would be impractical if the optimal solutions of GLB-RT required that requests from each source were divided up among all of the data centers. In general, each λ_{ij} could be nonzero in an optimal solution, yielding flows of requests from all sources to all data centers. In practice, this would lead to significant scaling issues. The sparsity of optimal solutions allows cloud providers to transform any optimal solution into a practically optimal solution.

Given long term procurement $\boldsymbol{q}^l$, how does it impacts on the operation of data centers, particularly the number of active servers m_i in data center i?

Theorem 3. *At any data center i, an optimal solution always utilizes the long term energy procurement q_i^l and renewable generation w_i^r as much as possible. It is simply represented by*

$$\begin{cases} m_i \geq w_i^r + q_i^l & \text{if } w_i^r + q_i^l < M_i \\ m_i = M_i & \text{if } w_i^r + q_i^l \geq M_i. \end{cases} \quad (5)$$

Proof. Appendix A.3. □

The theorem states that a data center i uses up the reserved electricity, including free renewable energy and pre-purchased electricity, to reduce the queueing delay cost. Implicitly, there is a trade-off between energy cost and queueing delay cost.

4 Predictability ~~analysis~~

We study the long-term predictability of metrics critical to our procurement systems for multi-timescale markets, such as workload, renewables, and electricity prices. The main results of our analysis are used as inputs for our proposed procurement systems and provide insights into the long-term prediction errors associated with each metric. We collected 3-year real-world traces of photovoltaic (PV) generation, wind generation, and electricity prices. The 3-year PV and wind generation data in 20 states of the US were downloaded via System Advisor Model (SAM) software, developed by the National Renewable Energy Laboratory (NREL) [1]. The 3-year electricity price data are from 20 cities of different regional transmission operators (RTOs) in the US, i.e. PJM, MISO, CAISO, ISONE, and NYSIO. In addition, we have 2-month workload data of 20 places in different US states, which are provided by Akamai Technologies that serves 15-30% of all Web content around the world from hundreds of data centers around the world [29].

In prior literature, prediction methods fall into one of the two categories: statistical methods and physical methods [21]. The statistical methods or time-series-based methods exploit the correlation of data in the temporal domain to predict the future from the past data. The statistical methods include linear and non-linear regression models [19], Kalman filter [27], and machine learning techniques [31, 36]. In the meantime, the physical methods use correlated physical conditions, such as geographical information, weather data, and time, to predict the future [37].

Long-term prediction is challenging for both statistical and physical methods. Statistical methods have to deal with the weak correlation between the past and future data. Meanwhile, physical methods require the input of physical features that are often not available for long-term prediction. For example, long-term weather forecast requires the data from many parts of the world which are only available in some specialized centers [30]. To improve the prediction accuracy, prediction methods may use the seasonality, such as the annual patterns. However, the effectiveness of using seasonality still heavily depends on the characteristics of data.

As the long-term forecaster is a part of our energy procurement system, it is necessary to design a long-term forecast method to produce the forecasted information for the energy procurement system. We design two long-term prediction methods, i.e. autoregressive (AR) and Support Vector Machine (SVM). While we use the AR method to capture daily patterns and the correlation between the past and future data, we develop SVM to include the seasonality of data. In particular, our AR model predicts the value $x(day + d\_ah, hr)$ at hour hr for d_ah day-ahead based on the past A days as $x(day + d\_ah, hr) = \sum_{a=0}^{A-1} \omega_a x(day - a, hr) + c$. The AR model can obtain the coefficients ω_a and constant c by fitting the model on the historical data. We observe that it is not necessary to pick a large value of A for long-term prediction because $A = 7$ already achieves a competitive performance. Additionally, d_ah is set at 30 days for PV generation, wind generation, and electricity price, and at 1 day for workload due to the limited length of data.

To utilize the seasonality of data, we design another long-term prediction method based on SVM. SVM is the learning algorithm that analyzes and makes the decision on the input data. Similar to the work [37], we focus the multiple classes of SVM. The first input of SVM is the average of the past A days. More importantly, the rest of inputs of SVM are the seasonality data, i.e., month of year, day of month, day of week, and hour of day [14]. For solar generation and wind generation, we expect to use *month of year*, *day of month*, and *hour of day* to capture their seasonality. Similarly, we use month of year, day of month, hour of day, and *day of week* in predicting electricity prices. As the limitation of the data length, only day of week and hour of day are used for predicting workload. The prediction range is set at the same as using the AR method, i.e., 30 days (solar generation, wind generation, and electricity prices), and 1 day (workload). The accuracy of SVM depends on the selection of SVM kernel functions, and the kernel parameter. For each set of data, we search for the best kernel function and the best kernel parameters based on LIBSVM [9]. The best kernel function is Radial Basis Function (RBF) but the kernel parameters vary for each set of data.

To quantify the performance of AR and SVM methods, prediction errors are used as a performance metric. Let $\hat{L}_j^r$, $\hat{w}_i^r$, and $\hat{p}_i^r$ denote long-term predicted values of renewable generation, workload, and electricity price. Fur-

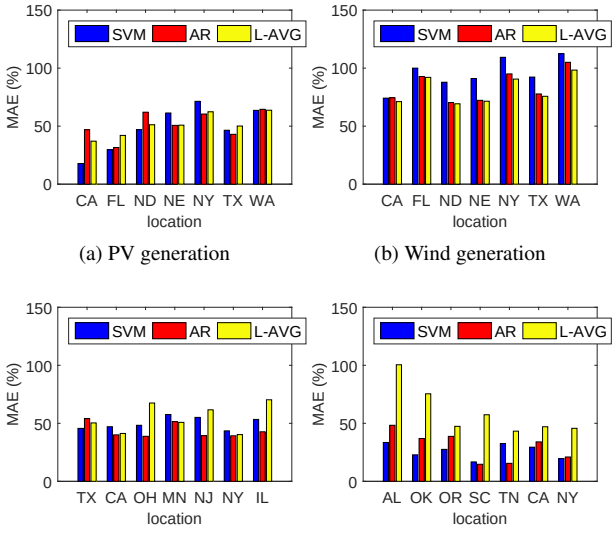

(a) PV generation (b) Wind generation

(c) Electricity price (d) Workload

Figure 3: Comparisons of SVM, AR and L-AVG. The codes of US states are California (CA), Florida (FL), North Dakota (ND), Nebraska (NE), New York (NY), Texas (TX), Washington (WA), Ohio (OH), Minnesota (MN), New Jersey (NJ), Illinois (IL), Alabama (AL), Georgia (GA), Oklahoma (OK), South Carolina (SC), Virginia (VA), and Tennessee (TN).

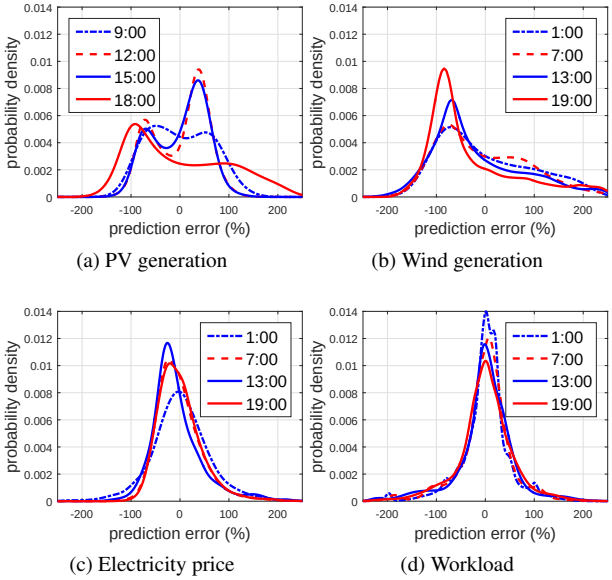

(a) PV generation (b) Wind generation

(c) Electricity price (d) Workload

Figure 4: Probability density of prediction errors at different time of the day.

ther, let

$$\varepsilon_i = w_i^r - \hat{w}_i^r, \tag{6a}$$

$$\xi_j = L_j^r - \hat{L}_j^r, \tag{6b}$$

$$\epsilon_i = p_i^r - \hat{p}_i^r, \tag{6c}$$

where ε_i, ξ_j, and ϵ_i are the prediction errors of renewable generation, workload, and electricity prices respectively. We normalize the prediction errors by the means of real values and show the values in percentage. For instance, if prediction error of PV generation is 20, then we underestimate the PV generation by 20% of the average PV generation.

To demonstrate the quality of the SVM and AR, we compare them with a baseline method, long-term average (L-AVG) [38]. L-AVG assumes that the long-term data has a long-term cycle. For example, PV generation may have a yearly cycle. In our model, we take the averages of 30 days of days at the same time in previous years for PV generation, wind generation, and electricity price. This enables us to capture the important seasonal patterns in the data as well. Assuming that user behaviors have weekly pattern, L-AVG take the averages of the workload demand at the same time of 7 days in the previous week. The mean absolute errors (MAE) of three methods are illustrated in Figure 3. In general, SVM and AR do not perform better than L-AVG in predicting solar and wind generation but they are better than L-AVG in predicting electricity price, and workload. SVM outperforms others methods in some states like California implying that the seasonality has more positive impact. Some states like Washington (WA) and New York (NY) having high precipitation can negatively affect the performance of SVM and AR predicting PV generation. Predicting wind generation is the hardest among the four types of data. It is because the wind generation has large very variation and fluctuation. SVM and AR are better than L-AVG in terms of predicting electricity prices. AR is surprisingly better than SVM in most states except for Texas (TX). The seasonality in real-time electricity prices is not strong enough to benefit SVM in long-term prediction. AR and SVM perform very well in predicting workload compared L-AVG in short-term. We also observe that the long-term prediction errors are relatively large compared to the mean of measured data. Via the performance of the three prediction methods, it is difficult to have a right method that works in the four types of data. The three methods do not show the significant performance gain to each other in long-term prediction Figure 3 also highlights that long prediction errors are locational dependent and depends on the nature of the predicted term.

As the performance of the AR method is competitive to the SVM and L-AVG methods, we investigate the prediction errors of the AR method. Figure 4 shows the probability density of the prediction errors at different times in a day. Each line represents the probability density of predic-

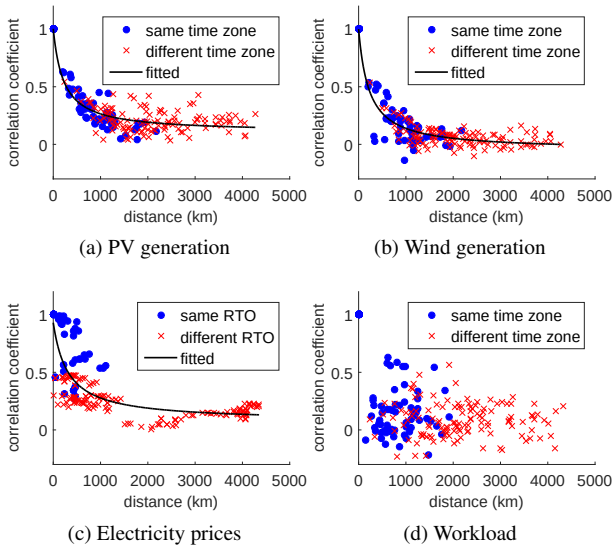

(a) PV generation (b) Wind generation

(c) Electricity prices (d) Workload

Figure 5: Correlation coefficients of prediction errors in spatial domain.

tion errors during an hour in a day. The probability densities are obtained by averaging the probability densities of all the collected data. Our first observation is that prediction errors have zero-mean. However, the probability densities of PV generation, wind generation, electricity price, and workload are asymmetric. In particular, our prediction algorithms tend to over-predict wind generation with high probability as shown by the peaks around -100 in Figure 4(b). This is because wind generation is often low. Meanwhile, the peaks of electricity price prediction errors are close to zero-mean. The prediction errors of workload are more likely to be symmetric and distributed around zero.

The correlation of prediction errors in spatial domain is of great interests to cloud providers with geo-distributed data centers. The correlation coefficients of prediction errors with respect to the distance between two locations are shown in Figure 5. We classify PV generation, wind generation, and workload into two groups: within the same time zone or different time zones. There are also two groups of electricity prices: within the same RTO or different RTOs. Figure 5 highlights that the distances have greater impact on the correlation than the groups have. In addition, the prediction errors of PV and wind generation are strongly correlated (greater than 0.5) within 500km, weakly correlated (less than 0.5) within 1000km, and almost independent to each other when more than 1500km apart. Note that electricity price is more correlated in spatial domain than PV generation and wind generation due to the fact that some of the prices can be generated by the same RTO. However, the prediction errors of workload are uncorrelated with respect to distances and groups. This is because workload depends on unpredictable user behaviors and the dynamic Internet conditions.

5 Algorithm Design

The energy procurement system needs algorithms for both energy procurement in long-term (EP-LT) and geographical load balancing in real-time (GLB-RT). Since GLB-RT is a deterministic convex optimization problem, it can be solved using standard convex programming algorithms. Thus, we focus on designing algorithms for energy procurement in the long-term markets. We design two algorithms, namely, Prediction based Algorithm (PA) and Stochastic Gradient estimate based Algorithm (SGA). PA is a heuristic algorithm that requires only the predicted mean values of renewable generations, workload, and electricity prices, whereas SGA is an optimal algorithm that requires the distributions of these quantities in addition to the mean values.

5.1 Prediction based Algorithm (PA)

Prediction based algorithm (PA) relies on the predicted mean values of renewable generation, workload, and electricity price. However, obtaining the mean values requires the knowledge of distribution of renewable generation, workload, and electricity price. Fortunately, the prediction errors are zero-mean as in our data analysis. Even though prediction errors are biased, we can simply adjust the prediction methods to eliminate the bias. Thus, the predicted values $\hat{L}_j^r$, $\hat{w}_i^r$, and $\hat{p}_i^r$ are approximately the prediction mean values of renewable generation, workload, and electricity price as shown in our data analysis.

To obtain the long term procurement $\boldsymbol{q}^l$, we simply solve the EP-LT and GLB-RT at the same time with all the random variables w_i^r, L_j^r, and p_i^r replaced by their predicted values as

$$\text{LT-PA: } \min_{\mathbf{m},\boldsymbol{\lambda},\mathbf{q}^l} \sum_{i=1}^{N} p_i^l q_i^l + \sum_{i=1}^{N} \hat{p}_i^r [m_i - \hat{w}_i^r - q_i^l]_+ + \beta \sum_i \sum_j h_{ij}(m_i, \lambda_{ij}),$$

subject to

$$\text{Constraints (1a)–(1e)}$$

$$q_i^l \geq 0 \; \forall i \in N.$$

The objective function of LT-PA is similar to that of the EP-LT without the expectation operation. The constraints over $\boldsymbol{m}$, $\boldsymbol{\lambda}$, and $\boldsymbol{q}^l$ of LT-PA are identical to those of the GLB-RT and EP-LT. LT-PA is a deterministic convex optimization problem and it can be efficiently solved [7].

5.2 Stochastic Gradient based Algorithm (SGA)

Although PA can offer a decision, the cloud providers would also want to have an algorithm that optimally procures electricity in long-term markets. To this end, we exploit the gradient characterization of the long-term objective (see Theorem 2) to design a stochastic gradient descent algorithm. The algorithm, namely, SGA, is summarized in Algorithm 1. The main idea of the algorithm is to compute a noisy estimate of the gradient of the long-term objective by averaging the gradient of the (random) total cost over a finite number of sample paths derived based on results in Section 4. This noisy gradient is used to perform a stochastic gradient descent. Stochastic approximation theory can then be used to prove convergence to the set of optimal solutions, as long as the step-size sequence is appropriately diminishing [20].

Algorithm 1 Stochastic Gradient based Algorithm (SGA).

Input: Obtain $\boldsymbol{p}^l$ from the $|N|$ long-term electricity markets.
Prepare $\mathbb{S}$ samples of $(\boldsymbol{w}^r, \boldsymbol{L}^r, \boldsymbol{p}^r)$ by using (6).
Output: $q_i^l \ \forall i \in N$
Initialize: $q_i^l = 0, \forall i \in N$.
Step: $\tau = 1$.
while 1 **do**
  for all k such that $1 \leq k \leq \mathbb{S}$ **do**
    Solve: GLB-RT for kth sample of $(\boldsymbol{w}^r, \boldsymbol{L}^r, \boldsymbol{p}^r)$ with long-term procurement $\boldsymbol{q}^l$
    Obtain: The Lagrange multipliers $\varrho_i^{(k)}$ corresponding to constraint (1f), $\forall i \in N$
  end for
  Compute: $\hat{\varrho}_i = \frac{1}{\mathbb{S}} \sum_{k=1}^{\mathbb{S}} \varrho_i^{(k)}, \forall i \in N$
  Update: $q_i^l = [q_i^l - \eta_\tau (p_i^l - \hat{\varrho}_i)]_{[0,M_i]}$ for $\forall i \in N$.
  Increase: $\tau = \tau + 1$.
end while

In the above algorithm, $[z]_{[0,M_i]}$ indicates the projection of z onto the set $[0, M_i]$.

Intuitively, assuming the gradient estimation is accurate enough, the algorithm is moving along the direction close to the steepest decent one. Therefore, the objective function decreases and the gradient $p_i^l - \hat{\varrho}_i$ becomes smaller. Eventually, $p_i^l - \hat{\varrho}_i$ approaches 0, q_i^l converges, and we obtain one optimal solution.

Indeed, we prove that SGA converges to the set of optimal solutions of EP-LT under the following standard assumption on the step-size sequence.

Assumption 1. $\sum_{\tau=1}^{\infty}(\eta_\tau) = \infty$ *and* $\sum_{\tau=1}^{\infty}(\eta_\tau)^2 < \infty$.

The convergence of SGA is asserted by the following theorem.

Theorem 4. *Under Assumption 1, almost surely, the iterates* $\boldsymbol{q}^l$ *generated by SGA converge to the set of optimal solutions of EP-LT as* $\tau \to \infty$.

We give the proof of Theorem 4 in Appendix B.

The bottleneck of SGA is the computation of the noisy gradient estimate, which involves solving $\mathbb{S}$ instances of GLB-RT. However, since this algorithm is used in long-term markets, its computation time would not be a bottleneck in practice.

6 Empirical evaluations

In this section, we perform several empirical studies to evaluate the proposed energy procurement system. We first illustrate the fast convergence of SGA to the optimal solution in Figure 6. Then we continue to highlight the cost savings by using our system in Figure 7. The impacts of renewable energy penetration level and prediction errors are also studied.

6.1 Experimental Setup

There are fourteen data centers in our system. They are located at 10 different states known to have Google data centers: California, Washington, Oregon, Illinois, Georgia, Virginia, Texas, Florida, North Carolina, and South Carolina. As we merge the data centers in each state, there are 10 logical data centers in our simulation, $N = 10$. We assume that there are one million servers distributed in ten logical data centers which can be half of the number of servers in Amazon Web Services (AWS) [28]. The peak power consumption for each server is 300W. We set the other parameters based on the baseline case of using the nearest routing technique where workload is just forwarded to the nearest data centers. The average workload is 30% of the total capacity of the data centers. As the network delays between sources and data centers are distance sensitive, π_{ij}, are estimated to be proportional to the distance between the centers of the two states [3]. The average network delays are 22 ms. The average queueing delays are 14.2 ms by based on the total arrival workload and the total capacity of data centers. The delay cost is computed based on the evidence that 100 ms latency costs 1% of Amazon in sales [22], and the total sale of AWS in 2015 reached 1.8 billion US dollars [13].

To compute the energy costs of the system, we assume that the system purchase the energy in long-term markets and real-time markets for an hour of operation. The electricity prices in real-time markets are the industrial electricity prices of each state in May 2010 [2]. Specifically, the mean values of real-time electricity prices, $\mathbb{E}[p_i^r]$, of considered states (cents per kWh) are as follows: 10.41 in California, 3.73 in Washington, 5.87 in Oregon, 7.48 in

Illinois, 5.86 in Georgia, 6.67 in Virginia 6.44 in Texas, 8.60 in Florida, 6.03 in North Carolina, and 5.49 in South Carolina. Since electricity prices in long-term markets are usually much cheaper than that of the real-time markets, we set $p_i^l = \frac{\mathbb{E}[p_i^r]}{2.5}$ for each data center i. Throughout this section, we set β = 1 meaning that delay cost and energy cost are equally important.

To simulate the uncertainties, the error distributions at 13 o'clock shown in Figure 4 are used to generate the samples of renewable energy generation (PV generation and/or wind generation), workload, and electricity price. The mean absolute errors (MAE) of prediction errors for PV generation, wind generation, electricity price, and workload demand are 45%, 65%, 40%, and 35%, respectively. The MAE are varied later to study the impacts of prediction errors. Wind generation is used as the renewable energy source by default. The penetration of the renewable energy is fixed at 50% of the averaged demand. We also vary the penetration of PV and wind generation to investigate the impacts of renewable portfolio and penetration level.

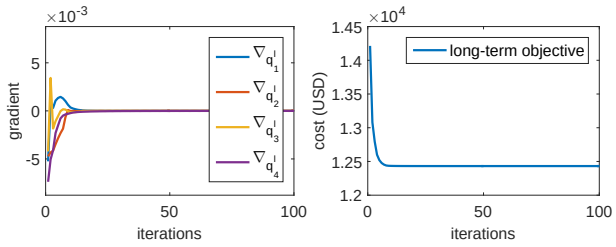

(a) Gradient components (b) Long-term objective

Figure 6: Convergence analysis.

Convergence Analysis Although SGEA is proved to converge eventually, it may not converge quickly in reality. The convergence speed mainly depends on how the step sizes are set. Stochastic optimization is known to have high computational complexity due to the large numbers of iterations and samples needed for each iteration. To reduce the number of iterations, we use the step size update rule as

$$\eta_t = \frac{s}{(S+t+1)^\alpha},$$

where s and S are non-negative constants and $0.5 < \alpha \leq 1$. This form fulfills the requirement of Assumption 1. Generally speaking, larger s can enhance the performance in the later iterations, but it may cause instability in the early iterations. Thus, S is used to prevent the instability. To speed up the convergence of algorithm, each gradient component has its own step-size, and the step-size is updated only if the gradient component switches from negative to positive or vise versa. Figure 6 illustrates four gradient components (of total ten) and the long-term objective function updated over iterations. As shown in the figure, gradient components and the long term objective $F^l(q^l)$ converge very quickly, i.e it is very close to the optimal value after merely 20 iterations. In reality, some gradient components $\nabla_{q_i^l}$ may converge to positive values. In such cases, the optimal solution has $q_i^l = 0$.

6.2 Cost savings

We highlight the benefit of our proposed system by comparing with the following algorithms.

No long-term procurement or geographical load balancing (nLTnGLB): nLTnGLB does not participate in long-term markets, i.e. $q_i^l = 0, \forall i \in N$, and the workload demand are forwarded to the closest data centers, a.k.a., nearest routing. We assume that the data centers activate all servers to minimize the queueing delay, i.e. $m_i = M_i$. Though simple, this policy is still widely used in practice.

Fixed long-term procurement without geographical load balancing (fLTnGLB): Cloud providers purchase a fixed amount of electricity ahead. We assume that the long-term procurement is 50% of workload mean. Like nLTnGLB, it uses nearest routing instead of GLB-RT.

No long-term procurement but with geographical load balancing (nLT): In this algorithm, we assume that the cloud provider does not purchase the energy in long term markets like nLTnGLB. However, the cloud provider executes GLB-RT to minimize the total cost in real-time.

Fixed long-term procurement geographical load balancing (fLT): fLT buys a fixed amount of electricity in long term markets same as fLTnGLB, i.e 50% of workload mean. In real-time markets, it executes GLB-RT.

In addition to the baseline algorithms, we compare our algorithms to an impractical algorithm, namely, **Oracle Algorithm (OA)**. OA assumes all realizations of renewable energy, workload, and electricity prices are fully known a-priori. Similarly to PA, the problem of EP-LT becomes an optimal deterministic problem. The cost of OA is measured by averaging its output over many realizations.

Figure 7 compares the cost performance among our proposed algorithms and the traditional algorithms. The figure highlight that our proposed algorithms PA and SGA save up to 44% compared to other simpler algorithms, and are comparable to the oracle algorithm OA, the impractical lower bound. It also shows the significant benefits for cloud providers to participate long-term markets. Surprisingly, PA achieves a very close performance compared with SGA. What are the intuitions behind this?

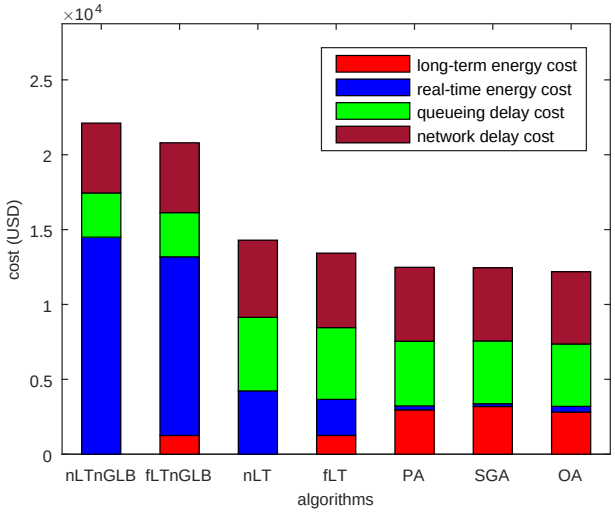

Figure 7: Cost comparison when $\beta = 1$ and 50 % renewable penetration.

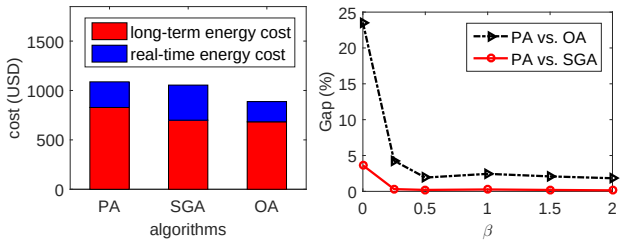

(a) $\beta = 0$ (b) Vary β

Figure 8: The impact of delay on the proposed algorithms. Without delay cost, there are significant gaps betwen PA, SGA, and OA.

Why does PA perform so well? Some intuitions behind the small cost performance gap between PA and SGA are the trade-off between energy cost and delay cost, and the compensation of GLB-RT at real-time markets. Specifically, PA is more aggressive in long-term markets, but its over-provisioned energy is used to reduce queuing delay. On the other hand, GLB utilizes the available renewable energy, and cheap electricity that compensate for performance gap caused by the prediction errors in long-term. In fact, the capability of GLB depends on multiple impact factors, such as renewable penetration rates, and the ratio of real-time prices to long-term prices. Hence, it is necessary to study the impact of these impact factors on the proposed algorithms.

How does the delay cost impact the proposed algorithms? We carry out the experiment of $\beta = 0$ in Figure 8a where the delay cost is ignored. The performance gap between PA and OA is 24% that is much larger than the gap (i.e. 2%) in Figure 7. As there is more space to improve the performance, SGA outperforms PA at 4% which can be a big revenue loss for the large-scale data centers. While PA is more aggressive in long-term markets, SGA is more conservative in long-term markets and buy more electricity in real-time markets. Figure 8b shows the cost performance gaps between PA versus OA and PA versus SGA. In general, the small values of β still have the significant impact on the proposed algorithms. The performance gaps sharply drop as β increases from 0 to 0.25 but it slight changes as β increases from 0.5 to 2. The impact of β on the performance gap proves that the trade-off between energy cost and delay cost makes the performance of PA performance very close to the optimal one.

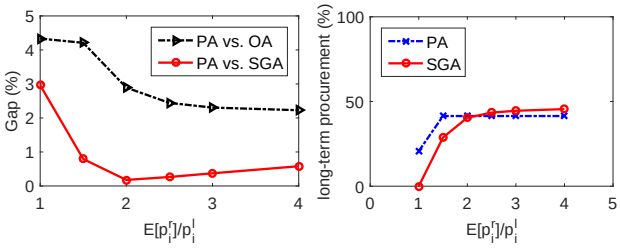

(a) PA vs. OA (b) Long term procurement

Figure 9: The impact of long-term prices on the proposed algorithms. The proposed algorithms are beneficial from the cheap long-term prices as they can be more agressive in long-term markets.

Impact of the ratio of real-time prices to long-term prices. We carry out another experiment that quantifies the impact of ratio of real-time prices to the long-term prices on our proposed algorithms in Figure 9. In this experiment, the long term prices are fixed, and we vary the real-time prices. Figure 9a shows the performance gap between PA versus SGA and PA versus OA. Intuitively, the cheap long-term prices allow the cloud providers to be more aggressive in long-term markets that explains why the gap between PA and OA is small as the ratio increases. However, the gap between PA and GA is very interesting. As the ratio goes up to 2, the gap becomes smaller but the gap increases as the ratio increases from 2 to 4. To explain this result, in Figure 9b illustrates the behaviors of PA and SGA in long-term markets. When the real-time prices are as cheap as the long-term prices, the aggressiveness in long-term results in more financial risk to the cloud providers. So, SGA is more conservative than PA when the ratio is low, i.e., less than 2. In contrast, SGA is more aggressive in long-term markets as the ratio becomes larger than 2.

Impacts of renewable energy. Renewable energy has been increasingly used to power data centers. Hence, we investigate the impacts of renewable energy integration on the our energy procurement system. We scale the penetra-

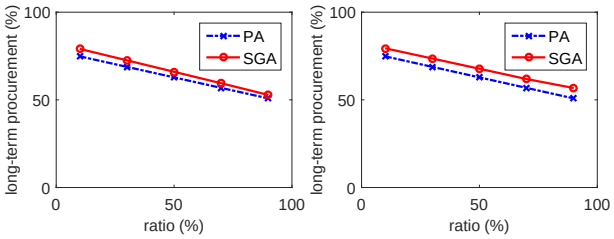

(a) PV penetration (b) Wind penetration

Figure 10: Impacts of renewable energy penetration levels on long-term energy procurement. SGA becomes more aggressive in the wind generation case than the PV generation case compared to PA.

tion levels of renewable energy from 5% to 95% of the total demand. We consider PV generation and wind generation as two main sources of renewable energy.

The impacts of renewable energy on the behaviors of PA and SGA are shown in Figure 10. Here, x-axis represents the penetration levels of renewable energy, and y-axis is the ratio (%) of total electricity purchased in long-term markets. PA performs similarly in both cases because it is only based on the predicted values. However, SGA is closer to PA in the PV generation case as the penetration of renewable energy increases, yet becomes more aggressive than PA in the wind generation case. The reason lies in the error distributions in Figure 4. While prediction errors of PV generation are concentrated on two peaks, the prediction errors of wind generation are centered around only one peak (around -100).

Impact of prediction errors. In this paper, we obtain the prediction errors from AR methods. However, different prediction methods may give different error distributions. Furthermore, as the prediction range varies from days to years, the MAEs of prediction also increases. Thus, we continue to study the impacts of error distributions and MAEs.

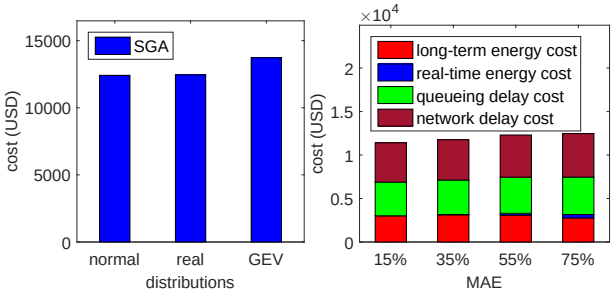

(a) Error distributions (b) Prediction errors

Figure 11: Impact of prediction on cost performance.

Figure ~~11 (a)~~ presents the cost of PA and SGA under three different error distributions, i.e. normal, "real", generalized extreme value (GEV) [11]. The normal distribution is symmetric around its mean. The GEV distribution is asymmetric and widely used in risk management and finance. We also add the distribution of AR prediction errors as the "real" distribution. The MAE of them are set at 35% for fair comparison. It is observed that the cost in normal distribution is the best among three error distributions, while GEV is the worst.

~~Figure 11 (b)~~ shows the cost of SGA with respect to different MAEs of "real" distribution. As the prediction errors increase, the real-time cost (real-time energy cost and delay cost) increase to compensate for the misprovisioning in long-term markets. Furthermore, the total cost slowly increases as the prediction errors increases. Again, the reasons behind this are the compensation of queueing delay cost over long-term energy cost and the independence of prediction errors.

7 Concluding remarks

Our work is the first systematic study of optimal energy procurement systems for geo-distributed data centers that utilize multi-timescale electricity markets. The contributions of this paper are three-fold: (i) designing algorithms for long-term electricity procurement; (ii) analyzing long-term prediction errors using real-world traces; and (iii) empirically evaluating the benefits of our proposed procurement systems. We proposed two algorithms, PA and SGA, both of which save up to 44% of the energy procurement cost compared to traditional algorithms that do not use long-term markets or geographical load balancing. While SGA provably converges to an optimal solution, PA surprisingly achieves a cost that is nearly optimal with much less computing effort.

There are a number of interesting directions for future research that are motivated by our work. In particular, generalizing our model to include more complicated forward contracts that procure energy that can be used over multiple time-slots is a challenging problem. Integrating storage capabilities, e.g., batteries and/or thermal storage, into the energy procurement optimization of multi-timescale markets is another challenging direction. There is no doubt that further research on how to optimally utilize multi-timescale markets will have a great impact on the future energy cost efficiency of Internet-scale services that use geo-distributed data centers.

References

[1] `https://sam.nrel.gov/`.

[2] http://www.eia.gov/.

[3] ATnT. U.s. network latency, 2016.

[4] L. M. Ausubel and P. Cramton. Using forward markets to improve electricity market design. *Utilities Policy*, 18(4):195–200, 2010.

[5] H. Beheshti and A. Croll. Performance impact: How web speed affects online business kpis. In *Velocity Online Conference*. O'Reilly, 2009.

[6] D. P. Bertsekas, A. Nedic, and A. Ozdaglar. *Convex analysis and optimization*. Athena Scientific, 2003.

[7] S. Boyd and L. Vandenberghe. *Convex optimization*. Cambridge university press, 2004.

[8] N. Buchbinder, N. Jain, and I. Menache. Online job-migration for reducing the electricity bill in the cloud. In *NETWORKING 2011*, pages 172–185. Springer, 2011.

[9] C.-C. Chang and C.-J. Lin. Libsvm: a library for support vector machines. *ACM Transactions on Intelligent Systems and Technology (TIST)*, 2(3):27, 2011.

[10] L. Chiaraviglio and I. Matta. An energy-aware distributed approach for content and network management. In *Computer Communications Workshops (INFOCOM WKSHPS), 2011 IEEE Conference on*, pages 337–342. IEEE, 2011.

[11] J. N. Corcoran. Modelling extremal events for insurance and finance. *Journal of the American Statistical Association*, 97(457):360–360, 2002.

[12] P. Cramton. Colombia's forward energy market. 2007.

[13] B. Darrow. Whoa: Amazon cloud sales up nearly 82% in second quarter, 2015.

[14] A. Deoras. Electricity load and price forecasting with matlab, 2010. [Online; accessed 25-April-2015].

[15] Google. Renewable energy, 2015. [Online; accessed 25-April-2015].

[16] M. Grant, S. Boyd, and Y. Ye. Cvx: Matlab software for disciplined convex programming, 2008.

[17] Y. Guo, Z. Ding, Y. Fang, and D. Wu. Cutting down electricity cost in internet data centers by using energy storage. In *Global Telecommunications Conference (GLOBECOM 2011), 2011 IEEE*, pages 1–5. IEEE, 2011.

[18] Y. Guo and Y. Fang. Electricity cost saving strategy in data centers by using energy storage. *Parallel and Distributed Systems, IEEE Transactions on*, 24(6):1149–1160, 2013.

[19] W. Guoyang, X. Yang, and W. Shasha. Discussion about short-term forecast of wind speed on wind farm. *Jilin Electric Power*, 181(5):21–4, 2005.

[20] H. J. Kushner and G. Yin. *Stochastic Approximation and Recursive Algorithms and Applications*. Springer, 2003.

[21] M. Lei, L. Shiyan, J. Chuanwen, L. Hongling, and Z. Yan. A review on the forecasting of wind speed and generated power. *Renewable and Sustainable Energy Reviews*, 13(4):915–920, 2009.

[22] J. Liddle. Amazon found every 100ms of latency cost them 1% in sales. *The GigaSpaces*, 27, 2008.

[23] M. Lin, A. Wierman, L. L. Andrew, and E. Thereska. Dynamic right-sizing for power-proportional data centers. *IEEE/ACM Transactions on Networking (TON)*, 21(5):1378–1391, 2013.

[24] Z. Liu, Y. Chen, C. Bash, A. Wierman, D. Gmach, Z. Wang, M. Marwah, and C. Hyser. Renewable and cooling aware workload management for sustainable data centers. In *ACM SIGMETRICS Performance Evaluation Review*, volume 40, pages 175–186. ACM, 2012.

[25] Z. Liu, M. Lin, A. Wierman, S. Low, and L. L. Andrew. Greening geographical load balancing. *IEEE/ACM Transactions on Networking (TON)*, 23(2):657–671, 2015.

[26] Z. Liu, M. Lin, A. Wierman, S. H. Low, and L. L. Andrew. Greening geographical load balancing. In *Proceedings of the ACM SIGMETRICS joint international conference on Measurement and modeling of computer systems*, pages 233–244. ACM, 2011.

[27] P. Louka, G. Galanis, N. Siebert, G. Kariniotakis, P. Katsafados, I. Pytharoulis, and G. Kallos. Improvements in wind speed forecasts for wind power prediction purposes using kalman filtering. *Journal of Wind Engineering and Industrial Aerodynamics*, 96(12):2348–2362, 2008.

[28] T. P. Morgan. A rare peek into the massive scale of aws. http://www.enterprisetech.com/2014/11/14/rare-peek-massive-scale-aws/. [Online; accessed 16-May-2016].

[29] E. Nygren, R. Sitaraman, and J. Sun. The Akamai Network: A platform for high-performance Internet applications. *ACM SIGOPS Operating Systems Review*, 44(3):2–19, 2010.

[30] W. M. Organization. Long range forecasting. https://www.wmo.int/pages/themes/climate/long_range_forecasting.php. [Online; accessed 16-May-2016].

[31] C. Paoli, C. Voyant, M. Muselli, and M.-L. Nivet. Forecasting of preprocessed daily solar radiation time series using neural networks. *Solar Energy*, 84(12):2146–2160, 2010.

[32] A. Qureshi, R. Weber, H. Balakrishnan, J. Guttag, and B. Maggs. Cutting the electric bill for internet-scale systems. In *ACM SIGCOMM computer communication review*, volume 39, pages 123–134. ACM, 2009.

[33] L. Rao, X. Liu, L. Xie, and W. Liu. Minimizing electricity cost: optimization of distributed internet data centers in a multi-electricity-market environment. In *INFOCOM, 2010 Proceedings IEEE*, pages 1–9. IEEE, 2010.

[34] L. Rao, X. Liu, L. Xie, and Z. Pang. Hedging against uncertainty: A tale of internet data center operations under smart grid environment. *Smart Grid, IEEE Transactions on*, 2(3):555–563, 2011.

[35] R. T. Rockafellar. *Convex analysis*. Princeton university press, 1970.

[36] A. Sfetsos and A. Coonick. Univariate and multivariate forecasting of hourly solar radiation with artificial intelligence techniques. *Solar Energy*, 68(2):169–178, 2000.

[37] N. Sharma, P. Sharma, D. Irwin, and P. Shenoy. Predicting solar generation from weather forecasts using machine learning. In *Smart Grid Communications (SmartGridComm), 2011 IEEE International Conference on*, pages 528–533. IEEE, 2011.

[38] G. Sinden. Characteristics of the uk wind resource: Long-term patterns and relationship to electricity demand. *Energy Policy*, 35(1):112–127, 2007.

[39] J. Whitney and P. Delforge. Data center efficiency assessment. *Issue paper on NRDC (The Natural Resource Defense Council)*, 2014.

[40] W. Zheng, K. Ma, and X. Wang. Exploiting thermal energy storage to reduce data center capital and operating expenses. In *High Performance Computer Architecture (HPCA), 2014 IEEE 20th International Symposium on*, pages 132–141. IEEE, 2014.

References

[1] https://sam.nrel.gov/.

[2] http://www.eia.gov/.

[3] ATnT. U.s. network latency, 2016.

[4] L. M. Ausubel and P. Cramton. Using forward markets to improve electricity market design. *Utilities Policy*, 18(4):195–200, 2010.

[5] H. Beheshti and A. Croll. Performance impact: How web speed affects online business kpis. In *Velocity Online Conference*. O'Reilly, 2009.

[6] D. P. Bertsekas, A. Nedic, and A. Ozdaglar. *Convex analysis and optimization*. Athena Scientific, 2003.

[7] S. Boyd and L. Vandenberghe. *Convex optimization*. Cambridge university press, 2004.

[8] N. Buchbinder, N. Jain, and I. Menache. Online job-migration for reducing the electricity bill in the cloud. In *NETWORKING 2011*, pages 172–185. Springer, 2011.

[9] C.-C. Chang and C.-J. Lin. Libsvm: a library for support vector machines. *ACM Transactions on Intelligent Systems and Technology (TIST)*, 2(3):27, 2011.

[10] L. Chiaraviglio and I. Matta. An energy-aware distributed approach for content and network management. In *Computer Communications Workshops (INFOCOM WKSHPS), 2011 IEEE Conference on*, pages 337–342. IEEE, 2011.

[11] J. N. Corcoran. Modelling extremal events for insurance and finance. *Journal of the American Statistical Association*, 97(457):360–360, 2002.

[12] P. Cramton. Colombia's forward energy market. 2007.

[13] B. Darrow. Whoa: Amazon cloud sales up nearly 82% in second quarter, 2015.

[14] A. Deoras. Electricity load and price forecasting with matlab, 2010. [Online; accessed 25-April-2015].

[15] Google. Renewable energy, 2015. [Online; accessed 25-April-2015].

[16] M. Grant, S. Boyd, and Y. Ye. Cvx: Matlab software for disciplined convex programming, 2008.

[17] Y. Guo, Z. Ding, Y. Fang, and D. Wu. Cutting down electricity cost in internet data centers by using energy storage. In *Global Telecommunications Conference (GLOBECOM 2011), 2011 IEEE*, pages 1–5. IEEE, 2011.

[18] Y. Guo and Y. Fang. Electricity cost saving strategy in data centers by using energy storage. *Parallel and Distributed Systems, IEEE Transactions on*, 24(6):1149–1160, 2013.

[19] W. Guoyang, X. Yang, and W. Shasha. Discussion about short-term forecast of wind speed on wind farm. *Jilin Electric Power*, 181(5):21–4, 2005.

[20] H. J. Kushner and G. Yin. *Stochastic Approximation and Recursive Algorithms and Applications*. Springer, 2003.

[21] M. Lei, L. Shiyan, J. Chuanwen, L. Hongling, and Z. Yan. A review on the forecasting of wind speed and generated power. *Renewable and Sustainable Energy Reviews*, 13(4):915–920, 2009.

[22] J. Liddle. Amazon found every 100ms of latency cost them 1% in sales. *The GigaSpaces*, 27, 2008.

[23] M. Lin, A. Wierman, L. L. Andrew, and E. Thereska. Dynamic right-sizing for power-proportional data centers. *IEEE/ACM Transactions on Networking (TON)*, 21(5):1378–1391, 2013.

[24] Z. Liu, Y. Chen, C. Bash, A. Wierman, D. Gmach, Z. Wang, M. Marwah, and C. Hyser. Renewable and cooling aware workload management for sustainable data centers. In *ACM SIGMETRICS Performance Evaluation Review*, volume 40, pages 175–186. ACM, 2012.

[25] Z. Liu, M. Lin, A. Wierman, S. Low, and L. L. Andrew. Greening geographical load balancing. *IEEE/ACM Transactions on Networking (TON)*, 23(2):657–671, 2015.

[26] Z. Liu, M. Lin, A. Wierman, S. H. Low, and L. L. Andrew. Greening geographical load balancing. In *Proceedings of the ACM SIGMETRICS joint international conference on Measurement and modeling of computer systems*, pages 233–244. ACM, 2011.

[27] P. Louka, G. Galanis, N. Siebert, G. Kariniotakis, P. Katsafados, I. Pytharoulis, and G. Kallos. Improvements in wind speed forecasts for wind power prediction purposes using kalman filtering. *Journal of Wind Engineering and Industrial Aerodynamics*, 96(12):2348–2362, 2008.

[28] T. P. Morgan. A rare peek into the massive scale of aws. `http://www.enterprisetech.com/2014/11/14/rare-peek-massive-scale-aws/`. [Online; accessed 16-May-2016].

[29] E. Nygren, R. Sitaraman, and J. Sun. The Akamai Network: A platform for high-performance Internet applications. *ACM SIGOPS Operating Systems Review*, 44(3):2–19, 2010.

[30] W. M. Organization. Long range forecasting. `https://www.wmo.int/pages/themes/climate/long_range_forecasting.php`. [Online; accessed 16-May-2016].

[31] C. Paoli, C. Voyant, M. Muselli, and M.-L. Nivet. Forecasting of preprocessed daily solar radiation time series using neural networks. *Solar Energy*, 84(12):2146–2160, 2010.

[32] A. Qureshi, R. Weber, H. Balakrishnan, J. Guttag, and B. Maggs. Cutting the electric bill for internet-scale systems. In *ACM SIGCOMM computer communication review*, volume 39, pages 123–134. ACM, 2009.

[33] L. Rao, X. Liu, L. Xie, and W. Liu. Minimizing electricity cost: optimization of distributed internet data centers in a multi-electricity-market environment. In *INFOCOM, 2010 Proceedings IEEE*, pages 1–9. IEEE, 2010.

[34] L. Rao, X. Liu, L. Xie, and Z. Pang. Hedging against uncertainty: A tale of internet data center operations under smart grid environment. *Smart Grid, IEEE Transactions on*, 2(3):555–563, 2011.

[35] R. T. Rockafellar. *Convex analysis*. Princeton university press, 1970.

[36] A. Sfetsos and A. Coonick. Univariate and multivariate forecasting of hourly solar radiation with artificial intelligence techniques. *Solar Energy*, 68(2):169–178, 2000.

[37] N. Sharma, P. Sharma, D. Irwin, and P. Shenoy. Predicting solar generation from weather forecasts using machine learning. In *Smart Grid Communications (SmartGridComm), 2011 IEEE International Conference on*, pages 528–533. IEEE, 2011.

[38] G. Sinden. Characteristics of the uk wind resource: Long-term patterns and relationship to electricity demand. *Energy Policy*, 35(1):112–127, 2007.

[39] J. Whitney and P. Delforge. Data center efficiency assessment. *Issue paper on NRDC (The Natural Resource Defense Council)*, 2014.

[40] W. Zheng, K. Ma, and X. Wang. Exploiting thermal energy storage to reduce data center capital and operating expenses. In *High Performance Computer Architecture (HPCA), 2014 IEEE 20th International Symposium on*, pages 132–141. IEEE, 2014.

A Proofs for Section 3

A.1 Proof of Theorem 1

To prove Theorem 1, we first show that the real-time objective is jointly convex with respect to $(\boldsymbol{q}^l, \boldsymbol{m}, \boldsymbol{\lambda})$.

Lemma 5. *$\tilde{F}^r$ as defined in* (2) *is jointly convex with respect to $(\boldsymbol{q}^l, \boldsymbol{m}, \boldsymbol{\lambda})$ over $\mathbb{R}_+^N \times C(L^r)$.*

Proof. We rewrite

$$\tilde{F}^r(\boldsymbol{q}^l, \boldsymbol{m}, \boldsymbol{\lambda}, \boldsymbol{p}^r, \boldsymbol{w}^r) = \sum_{i=1}^N p_i^l[m_i - w_i^r - q_i^l]_+ + \beta \sum_{i=1}^N \frac{\lambda_i}{\mu_i - \lambda_i/m_i} + \beta \sum_{i=1}^N \sum_{j=1}^J \lambda_{ji}\pi_{ij}. \quad (8)$$

Since $m_i - w_i^r - q_i^l$ is an affine function, and $[\cdot]_+$ is convex and non-decreasing, $\sum_{i=1}^N p_i^l[m_i - w_i^r - q_i^l]_+$ is jointly convex with respect to $(\boldsymbol{q}^l, \boldsymbol{m})$.

Here, we need to show that $\sum_{i=1}^N \frac{\lambda_i}{\mu_i - \lambda_i/m_i}$ is jointly convex with respect to (m_i, λ_i). We have $\frac{\bar{\lambda}_i}{\mu_i - \bar{\lambda}_i}$ is non-decreasing and convex in $0 \le \bar{\lambda}_i \le \mu_i$, and $\bar{\lambda}_i = \lambda_i/m_i$ is convex over $\lambda_i \ge 0$ and $m_i \ge 0$. So, $\frac{\lambda_i/m_i}{\mu_i - \lambda_i/m_i}$ is convex. In addition, m_i is non-negative so $\frac{\lambda_i}{\mu_i - \lambda_i/m_i}$ is convex because the perspective of a convex function is convex [7]).

Since $\lambda_i = \sum_j \lambda_{ij}$ is linear and non-decreasing, $\frac{\sum_j \lambda_{ij}}{\mu_i - (\sum_j \lambda_{ij})/m_i}$ is convex. Thus, $\tilde{F}^r$ is jointly convex with respect to $(\boldsymbol{q}^l, \boldsymbol{m}, \boldsymbol{\lambda})$ because the summation of convex functions are convex. □

of Theorem 1. From Lemma 5, we know that the real time objective function $\tilde{F}^r(\boldsymbol{q}^l, \boldsymbol{m}, \boldsymbol{\lambda}, \boldsymbol{p}^r, \boldsymbol{w}^r)$ is jointly convex with respect to $(\boldsymbol{q}^l, \boldsymbol{m}, \boldsymbol{\lambda})$. It then follows that

$$F^{*r}(\boldsymbol{q}^l, \boldsymbol{p}^r, \boldsymbol{L}^r, \boldsymbol{w}^r) = \min_{(\boldsymbol{m}, \boldsymbol{\lambda}) \in C(L^r)} \tilde{F}^r(\boldsymbol{q}^l, \boldsymbol{m}, \boldsymbol{\lambda}, \boldsymbol{p}^r, \boldsymbol{w}^r)$$

is convex with respect to $\boldsymbol{q}^l$ (see [7]). Finally, since the expectation operation preserves convexity, we conclude that $F^l(\boldsymbol{q}^l)$ is convex with respect to $\boldsymbol{q}^l$. □

A.2 Proof of Theorem 2

This section is devoted to the proof of Theorem 2. To prove Theorem 2, it suffices to show that

$$\frac{\partial \mathbb{E}\left[F^{*r}(\boldsymbol{q}^l, \boldsymbol{p}^r, \boldsymbol{L}^r, \boldsymbol{w}^r)\right]}{\partial q_i^l} = \mathbb{E}\left[\frac{\partial F^{*r}(\boldsymbol{q}^l, \boldsymbol{p}^r, \boldsymbol{L}^r, \boldsymbol{w}^r)}{\partial q_i^l}\right] = -\mathbb{E}\left[\varrho_i(\boldsymbol{q}^l, \boldsymbol{p}^r, \boldsymbol{L}^r, \boldsymbol{w}^r)\right]. \quad (9)$$

The first step is to prove that the Lagrange multiplier of GLB-RT corresponding to the constraint (1f) is unique.

Lemma 6. *With probability 1, GLB-RT has a unique Lagrange multiplier, denoted $\varrho_i(\boldsymbol{q}^l, \boldsymbol{p}^r, \boldsymbol{L}^r, \boldsymbol{w}^r)$, corresponding to the constraint* (1f)*.*

Proof. In this proof, for notational simplicity, we suppress the dependence of the primal and dual solutions of GLB-RT on $(\boldsymbol{q}^l, \boldsymbol{p}^r, \boldsymbol{L}^r, \boldsymbol{w}^r)$. Consider a primal solution of GLB-RT $(\boldsymbol{q}^r, \boldsymbol{m}, \boldsymbol{\lambda})$ with $\boldsymbol{m} > 0$. Such a solution exists with probability 1, since $\boldsymbol{w}^r > 0$ with probability 1.

Now any dual solution must satisfy the KKT conditions. This implies the following conditions. (Since the constraint $\lambda_i \le m_i\mu_i$ is never binding, the corresponding Lagrange multiplier $\sigma_i = 0$ and does not feature in the following.)

$$-\beta\left(\frac{\frac{\lambda_i}{m_i}}{\mu_i - \frac{\lambda_i}{m_i}}\right)^2 + \bar{\omega}_i - \underline{\omega}_i + \varrho_i = 0 \quad (10)$$

$$\bar{\omega}_i(m_i - M_i) = 0; \bar{\omega}_i \ge 0, m_i \le M_i \quad (11)$$

$$\underline{\omega}_i m_i = 0; \underline{\omega}_i \ge 0, m_i \ge 0 \quad (12)$$

$$p_i^r - \kappa_i - \varrho_i = 0 \quad (13)$$

$$\kappa_i q_i^r = 0; \kappa_i \ge 0, q_i^r \ge 0 \quad (14)$$

$$\varrho_i(-q_i^r + m_i - w_i^r - q_i^l) = 0; \quad (15)$$

$$\varrho_i \ge 0, q_i^r \ge m_i - w_i^r - q_i^l \quad (16)$$

We now argue that ϱ_i is unique for all i. Consider the following two cases.

Case 1: $w_i^r + q_i^l > M_i$. In this case, it follows that $m_i < w_i^r + q_i^l + q_i^r$. Using (15), we conclude that $\varrho_i = 0$.

Case 2: $w_i^r + q_i^l < M_i$. Here we consider two sub-cases.

Case 2a: $m_i = M_i$. In this case, it follows that $q_i^r > 0$, which implies that $\kappa_i = 0$ (by (14)). Thus, we have, using (13), that $\varrho_i = p_i^r$.

Case 2b: $m_i < M_i$. In this case, since $m_i \in (0, M_i)$, we have $\bar{\omega}_i = \underline{\omega}_i = 0$ (by (11) and (12)). Thus, from (10), we have

$$\varrho_i = \beta\left(\frac{\frac{\lambda_i}{m_i}}{\mu_i - \frac{\lambda_i}{m_i}}\right)^2.$$

Since the event $w_i^r + q_i^l = M_i$ has zero probability, we may ignore this case. This completes the proof. □

Given Lemma 6, it follows from standard sensitivity analysis in convex optimization (see Section 6.5.3 and

6.5.4 in [6]) that

$$\frac{\partial F^{*r}(\boldsymbol{q}^l, \boldsymbol{p}^r, \boldsymbol{L}^r, \boldsymbol{w}^r)}{\partial q_i^l} = -\varrho_i(\boldsymbol{q}^l, \boldsymbol{p}^r, \boldsymbol{L}^r, \boldsymbol{w}^r). \quad (17)$$

This proves the second equality in (9). Thus, to complete the proof of Theorem 2, it only remains to justify the interchange of the partial derivative and the expectation in the first equality. We justify this interchange by invoking the dominated convergence theorem as follows.

Let e_i denote a column vector in $\mathbb{R}^N$, with 1 in the ith entry and 0 elsewhere.

Lemma 7. *For any $\delta \neq 0$ and $i \in N$,*

$$\left| \frac{F^{*r}(\boldsymbol{q}^l + \delta e_i, \boldsymbol{p}^r, \boldsymbol{L}^r, \boldsymbol{w}^r) - F^{*r}(\boldsymbol{q}^l, \boldsymbol{p}^r, \boldsymbol{L}^r, \boldsymbol{w}^r)}{\delta} \right| \leq p_i^r.$$

Proof. It is easy to see that

$$F^{*r}(\boldsymbol{q}^l, \boldsymbol{p}^r, \boldsymbol{L}^r, \boldsymbol{w}^r) \leq \delta p_i^r + F^{*r}(\boldsymbol{q}^l + \delta e_i, \boldsymbol{p}^r, \boldsymbol{L}^r, \boldsymbol{w}^r).$$

The statement of Lemma 7 follows from the fact that the function $F^{*r}(\boldsymbol{q}^l + \delta e_i, \boldsymbol{p}^r, \boldsymbol{L}^r, \boldsymbol{w}^r)$ is non-increasing with respect to δ. □

Since $\mathbb{E}[p_i^r] < \infty$, it follows from the dominated convergence theorem that

$$\mathbb{E}\left[\lim_{\delta \to 0} \frac{F^{*r}(\boldsymbol{q}^l + \delta e_i, \boldsymbol{p}^r, \boldsymbol{L}^r, \boldsymbol{w}^r) - F^{*r}(\boldsymbol{q}^l, \boldsymbol{p}^r, \boldsymbol{L}^r, \boldsymbol{w}^r)}{\delta}\right]$$
$$= \lim_{\delta \to 0} \frac{\mathbb{E}\left[F^{*r}(\boldsymbol{q}^l + \delta e_i, \boldsymbol{p}^r, \boldsymbol{L}^r, \boldsymbol{w}^r)\right] - \mathbb{E}\left[F^{*r}(\boldsymbol{q}^l, \boldsymbol{p}^r, \boldsymbol{L}^r, \boldsymbol{w}^r)\right]}{\delta}.$$

This proves the first equality in (9), and completes the proof of the theorem.

A.3 Proof of Theorem 3

We assume there an optimal solution S such that $\lambda_i > 0$ and $0 < m_i < w_i^r + q_i^l$. $\lambda_i = 0$ or $m_i = 0$ is not ignored because it is equivalent to shutting down data center i. Here, $\underline{\omega}_i = \varrho_i = 0$.

If $w_i^r + q_i^l < M_i$ and $m_i < w_i^r + q_i^l$, $\bar{\omega}_i = 0$. $\bar{\omega}_i = \underline{\omega}_i = \varrho_i = 0$ results in λ_i / m_i becomes zero as (10). $\lambda_i = 0$ or $m_i = \infty$ contradicts the assumption. So, $m_i \geq w_i^r + q_i^l$ if $w_i^r + q_i^l < M_i$.

If $w_i^r + q_i^l \geq M_i$, we assume that $m_i < M_i$. $\bar{\omega}_i = \underline{\omega}_i = \varrho_i = 0$ again leads to the contradiction to the assumption. So, $m_i = M_i$ if $w_i^r + q_i^l \geq M_i$.

B Convergence of SGA

This section is devoted to the proof of Theorem 4. Invoking Theorem 2.1 in [20], the almost sure convergence of the iterates of SGA to the set of optimal solutions of EP-LT holds if the following two conditions are satisfied.

1. $\nabla F^l : \mathbb{R}_+^N \to \mathbb{R}^N$ is continuous.
2. $\sup_{q^l \in \mathbb{R}_+^N} \mathbb{E}\left[(\varrho_i(\boldsymbol{q}^l, \boldsymbol{p}^r, \boldsymbol{L}^r, \boldsymbol{w}^r))^2\right] < \infty$.

Condition (1) above holds since the gradient of a differentiable convex function is convex; see Theorem 25.5 in [35]. Condition (2) holds since

$$\varrho_i(\boldsymbol{q}^l, \boldsymbol{p}^r, \boldsymbol{L}^r, \boldsymbol{w}^r) \leq p_i^r$$

(see (17) and Lemma 7). This completes the proof.